Journal of Materials Chemistry C

ROYAL SOCIETY OF CHEMISTRY

PAPER

View Article Online
View Journal | View Issue



Cite this: J. Mater. Chem. C, 2023, 11, 2600

# Gold nanocluster decorated fibrous substrate for photo-modulated cellular growth†

Bowen Li, [a] Yuetong Kang, [a] Xiaoyu Wang, *[a] Pengbo Zhang [b] and Lidong Li *[a]

Received 6th December 2022,
Accepted 17th January 2023

DOI: 10.1039/d2tc05194j

rsc.li/materials-c



Three-dimensional substrates with nanostructures have drawn attention in biological fields, especially in cell cultures. A photothermal effect is introduced into the substrate to realize remote regulation of cellar behaviours, which is highly desirable. Herein, we report a photofunctional fibrous substrate by decorating photothermal gold nanoclusters to modulate cell growth. Through programmable annealing, the ultra-small Au NCs were well integrated into the filamentous aggregates of gellan gum. Benefiting from the metal coordination interactions in biomolecules, a fibrous substrate that consists of gold nanoclusters, filamentous aggregates of gellan gum and bioactive whey protein were obtained *via* ionic crosslinks. The incorporated gold nanoclusters tightened the arrangement of the fibrous structures and increased the rigidity of the substrate. The enhanced local mechanical property was found to promote cell adhesion. Meanwhile, the photothermal properties of gold nanoclusters permitted whey protein release from the substrate by light in an on-demand way. The released whey protein significantly induced cell proliferation. Therefore, photo-modulated cellular growth was achieved on the gold nanocluster decorated fibrous substrate. Coupling optical gold nanoclusters in a three-dimensional substrate can facilely introduce light responsiveness, which will broaden their biomedical applications.

## 1. Introduction

The cellular microenvironment, especially the extracellular matrix, plays an important role for multicellular organisms.[1–3] The extracellular matrix is a three-dimensional fibrous substrate that is composed of fibrin, collagen, proteoglycans, glycosaminoglycan and growth factors.[4] The substrate not only provides physical support for cells, but also its mechanical structures and intrinsic bioactive molecules can directly determine cellular behaviour in tissue development from the nanoscale to the macroscale.[5,6] Therefore, the extracellular-matrix-inspired biomimetic platform has been developed to regulate cellular fate and further advance tissue repair and regeneration.[7,8] Biomaterials, such as collagen, polysaccharide, and peptide amphiphiles can self-assemble into nanofibers to form fibrous substrates.[9–11] Moreover, these assemblies can be structurally designed due to the biomolecular structure.[12] The metal-coordination bonds can be easily introduced to increase the extent of crosslinking, which has potential for improving the architectural strength.[13–15] Self-assembled fibrous substrates with tunable mechanical properties enable the mimicry of structural features of the extracellular matrix to provide mechanical cues.

Moving beyond the morphology to regulate cellular behaviour, incorporating controllable bioactive cues to mimic the extracellular matrix can enhance the biological performance of the artificial substrate.[16,17] Among them, growth factors, inhibitors, and bone morphogenetic proteins have been loaded to modulate cellular growth and proliferation.[18–20] To achieve a better regulation effect, the loaded bioactive substances are expected to release at the desired time and location. Light, which is regarded as a non-invasive stimulus, can introduce a photothermal effect, which offers on-demand spatiotemporal control over substrate properties for releasing bioactive substances.[21–24] Thus, this necessarily requires the integration of the photothermal material into the substrate.

Organic conjugated polymers and inorganic nanoparticles have been integrated into the design of artificial substrates for producing light-responsive properties.[25–32] Gold nanoclusters (Au NCs) consist of a certain number of gold atoms and organic ligands, which feature discrete energy levels and quasi-molecular electronic character.[33–35] Au NCs can be structurally tailored to exhibit good photothermal properties *via* non-emissive transition, which is different from the conventional surface plasma effect of larger-sized gold nanostructures.[36–39] In addition, the photothermal effect of Au NCs can parallel to gold nanorods.[40]

[a] State Key Laboratory for Advanced Metals and Materials, School of Materials Science and Engineering, University of Science and Technology Beijing, Beijing 100083, P. R. China. E-mail: wangxy@ustb.edu.cn, lidong@mater.ustb.edu.cn
[b] School of Chemistry and Biological Engineering, University of Science and Technology Beijing, Beijing 100083, P. R. China

† Electronic supplementary information (ESI) available. See DOI: https://doi.org/10.1039/d2tc05194j

Moreover, the ultra-small size (~2 nm) may permit the doping of Au NCs with good dispersion and without interference to the intrinsic structure of the artificial substrate.[41,42] Meanwhile, with the selected biomolecules as organic ligands, Au NCs can assemble with the artificial substrate noncovalently, readily avoiding complex chemical links.[43–45] Therefore, customized Au NCs with good biocompatibility show promising potential in the smart release of bioactive substances.

Herein, we have incorporated photothermal Au NCs with pre-annealed gellan gum *via* ionic crosslink to develop a smart nanofibrous substrate for light-modulated cellular growth. As illustrated in Fig. 1a, during the annealing process, the chain conformation of gellan gum underwent a helical transition by intermolecular hydrogen bonding, which subsequently strengthened the interchain entanglement. Glutathione-protected Au NCs were selected as the photothermal agents. The abundant carboxyl groups that exist in glutathione ligands enable the Au NCs to be efficiently crosslinked by calcium ions ($Ca^{2+}$). Thereby, the physical integrity between them and the tight binding of the gellan gum helices formed a light-responsive nanofibrous substrate (fibrous-Au-GG). The linked ultra-small Au NCs did not alter the fibrous structure, but rather increased the stiffness to promote cell adhesion. After loading whey proteins as the bioactive substances, the light-generated heat derived from the Au NCs offered the smart substrate to transiently release whey proteins, which enhanced cellular growth (Fig. 1b). Thus, we developed an optical functional system incorporating structural and bioactive cues to modulate cellular growth.

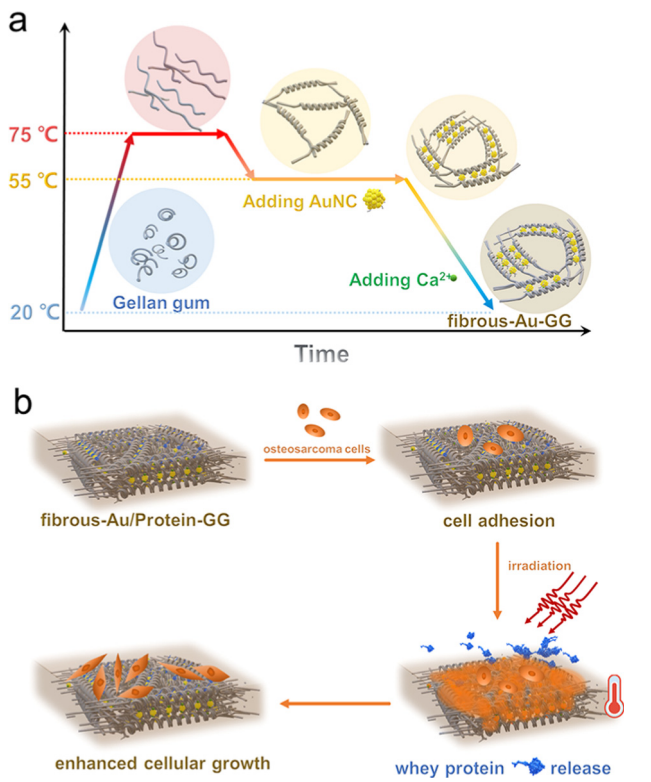


Fig. 1 Schematic illustrations on (a) the preparation of the nanofibrous substrate by ionic crosslinked photothermal Au NCs with pre-annealed gellan gum and (b) the processes of cell adhesion on the nanofibrous substrate and the photothermal responsive protein release for enhancing cellular growth.

## 2. Experimental

### 2.1 Materials and methods

Reduced L-glutathione, hydrogen tetrachloroaurate(III) trihydrate ($HAuCl_4 \cdot 3H_2O$), calcium chloride and 3-(4,5-dimethylthiazol-2-yl)-2,5-diphenyltetrazolium bromide (MTT) were purchased from Sigma-Aldrich. Gellan gum, penicillin-streptomycin mixed solution and phosphate buffer (pH 7.4) were purchased from Beijing BioDee Biotechnology Co., Ltd. MG-63 human osteosarcoma cells were purchased from the Chinese Academy of Medical Sciences. Minimum essential media (MEM), fetal bovine serum (FBS), glutamine, and calcein acetoxymethyl ester/propidium iodide (calcein-AM/PI) stain kit were purchased from Beijing Solarbio Science & Technology Co., Ltd. Whey proteins and fluorescein isothiocyanate-labelled whey proteins (FITC-whey protein) were purchased from QIYUEBIO Co., Ltd. Other chemicals were purchased from Beijing Chemical Company. All chemicals were used as received.

Transmission electron microscopy (TEM) images of the Au NCs were taken on air-dried carbon-coated copper grids by a JEMO 2010 electron microscope. Scanning electron microscopy (SEM) images and element analysis of the fibrous substrates and hydrogels were taken in secondary electron mode by a SUPRA55 electron microscope with energy-dispersive X-ray spectrometry. It was necessary to snap-freeze the samples with liquid nitrogen to preserve their forms and to freeze-dry them to remove water. All the samples were sprayed with platinum for SEM imaging. X-ray photoelectron spectra (XPS) were taken on an AXIS Ultra DLD spectrometer. UV-Vis spectra and fluorescence spectra were taken on a Hitachi U-3900H spectrophotometer and a Hitachi F-7000 spectrometer, respectively. The compression moduli of the substrates were determined by a universal testing machine (WDW-1, China). The diameters of these substrates were 3 cm. The surface roughness of the fibrous substrates and hydrogels were determined by a 3D laser scanning microscope (Keyence, VK-X150). Irradiation was conducted by a 660 nm laser generator (Changchun LS Optoelectronic Technology). The temperature change under 660 nm irradiation was monitored by a Fluke Ti400 infrared imager. The fluorescence images were taken by an Olympus 1 × 73 fluorescence microscope. The absorbance at 570 nm for MTT analysis was collected by a BIO-TEK Synergy HT microplate reader.

### 2.2 Preparation of fibrous substrates and hydrogels

Glutathione protected Au NCs were prepared by reduction of $HAuCl_4$ according to our published procedure.[46] The concentration of the Au NCs was fixed to 10 mg $mL^{-1}$. The 0.3 g gellan gum was added to 19 mL water and the mixture was heated to 75 °C to obtain the GG gellan gum solution. After cooling to 55 °C, 1 mL of solution containing 3 mg of Au NCs was added. Each 4.5 mL of the solution was added to each well of a 6-well

plate. The plate was quickly placed in an oven at 50 °C for 5 hours. Then, 2 mL of calcium chloride (0.3 M) was added to each well and was left for 20 min to obtain fibrous-Au-GG. 0.3 g of gellan gum was added to 20 mL of water to obtain fibrous-GG in the same way. After the gellan gum solution was cooled to 55 °C, 1 mL of the solution containing 3 mg of Au NCs and 2 mg whey protein was added. Then, the whey protein loaded fibrous-Au-GG (named fibrous-Au/protein-GG) was prepared in the same way. FITC-whey protein replaced the whey protein to prepare the same substrate.

Without putting it into the oven, the mixture of Au NCs and gellan gum was cooled to room temperature. Then, 2 mL of calcium chloride (0.3 M) was added to each well to obtain the Au-GG hydrogel. The Au/protein-GG hydrogel was prepared in the same way. A pure gellan gum solution was used to prepare the GG hydrogel.

All the samples were immersed into water for 12 h to remove any unfixed components.

### 2.3 Photothermal property measurements

The fibrous substrates including fibrous-GG, fibrous-Au-GG and fibrous-Au/protein-GG were irradiated by a 660 nm laser with the power of 1.65 W $cm^{-2}$, respectively. After 30 min, the laser was turned off. The *in situ* temperature change at the irradiation point of the sample was recorded by an infrared imager every 15 s.

Two milliliters of water containing fibrous-Au-GG were irradiated by a 660 nm laser with the power of 1.65 W $cm^{-2}$. The photothermal heating-cooling curves of water were obtained, which were used to calculate the photothermal conversion efficiency according to the published procedure.[47,48]

### 2.4 Protein release in the fibrous substrate

FITC-whey protein was used as a model protein to prepare fibrous-Au/protein-GG. One set of fibrous-Au/protein-GG was immersed into 2 mL of PBS for 30 min. The emission intensities of FITC from fibrous-Au/protein-GG and the PBS were measured at an interval of 3 min. Another set of fibrous-Au/protein-GG was irradiated by a 660 nm laser. The fluorescence intensities of FITC were measured in the same way.

### 2.5 Cell adhesion and proliferation assay

MG-63 cells were cultured in MEM supplemented with 10% fetal bovine serum, 2 mM glutamine, and 100 μg per mL penicillin–streptomycin mixture. Different fibrous substrates and hydrogels were placed in a 96-well plate. The $5 \times 10^3$ MG-63 cells were seeded on each substrate and incubated for 12 h. The loaded whey proteins were not labelled with FITC. For the cell adhesion assay, each well of the cells were washed with PBS three times and were stained with calcein AM/PI for 15 min. The green fluorescence from calcein AM and the red fluorescence from PI from the cells were collected.

For the cell proliferation assay, after cellular adherence to the fibrous substrates, 660 nm light with the power density of 0.81 W $cm^{-2}$ was applied to irradiate the sample. After irradiation for 30 min, the cells were incubated for one day. The cells were washed with PBS and were stained with calcein AM/PI for observation. To evaluate the cell viability, after one day of cell incubation, 100 μL of 0.5 mg $mL^{-1}$ MTT replaced the medium. After 4 h of incubation, 100 μL of dimethyl sulfoxide was added to dissolve the reduced formazan. The absorbance at 570 nm was measured after removing the different substrates.

## 3. Results and discussion

Carboxyl-rich gellan gum was selected as the substrate because of its resemblance to glycosaminoglycan of the extracellular matrix. Through annealing, filamentous structures were formed in the gellan gum based on hydrogen bonds.[10,49] The Au NCs were first prepared. Their average size was determined by counting 100 Au NCs from a high-resolution TEM image. The Au NCs, featuring a diameter of ~2 nm and a (111) face-centred cubic structure with 2.3 Å interplanar spacing (Fig. 2a), were then added during the annealing process of the gellan gum solution. The stable coordination between the carboxyl group and $Ca^{2+}$ permit the crosslinking between the glutathione-protected Au NCs and the gellan gum, and then the formation of fibrous-Au-GG. As the SEM image in Fig. 2b shows, the surface of fibrous-Au-GG structure displayed ordered structures of filamentous aggregates like elongated fibers. The cross-section image shows a network structure without large pores, which was induced by the crosslinking of these filamentous aggregates (Fig. 2c). In order to investigate the presence of the Au NCs, an elemental mapping analysis was conducted. As shown in Fig. 2d, the Au elements were well distributed in fibrous-Au-GG. The gellan gum was annealed without loading the Au NCs to obtain fibrous-GG. No Au element was detected in fibrous-GG (Fig. S1, ESI†). The similar network structure was obtained, but the pores were much bigger. And the filamentous aggregates were looser than fibrous-Au-GG (Fig. S2, ESI†). It is probably due to the absence of inorganic Au NCs. To some extent, the Au NCs hinder the further aggregation of the filamentous aggregates. After loading the Au NCs, fibrous-Au-GG showed a brown colour, which differed from the semi-transparent fibrous-GG (Fig. S3, ESI†). These results demonstrated the successful loading of the Au

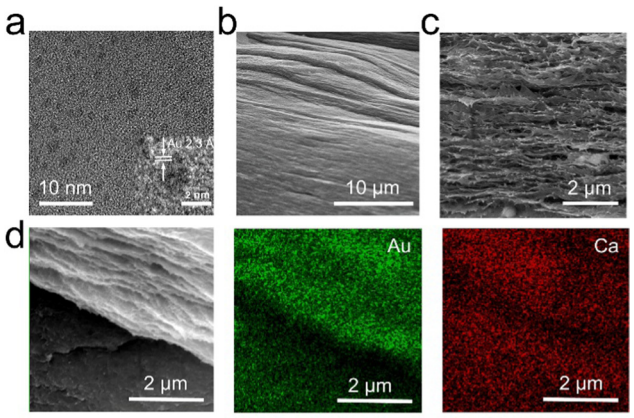


Fig. 2 (a) TEM images of photothermal Au NCs. Insert: Magnified TEM image (scale bar, 2 nm). (b) The surface and (c) cross-section SEM images of fibrous-Au-GG. (d) Au and Ca elemental mapping images of fibrous-Au-GG.

 

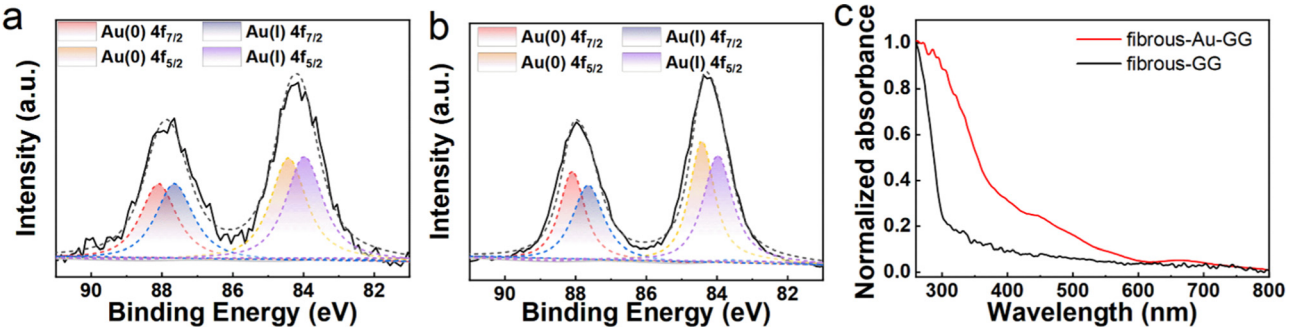


Fig. 3 The XPS spectra of the Au 4f orbital in (a) fibrous-Au-GG and (b) Au NCs. (c) Normalized absorption spectra of fibrous-GG and fibrous-Au-GG.



NCs in fibrous-Au-GG. The simultaneous distribution of Ca and Au elements in fibrous-Au-GG proved the immobilization of the Au NCs with $Ca^{2+}$.

Furthermore, the binding energies of Au 4f for fibrous-Au-GG were located at about 87.95 and 84.20 eV (Fig. 3a), which are between those for Au(0) and Au(I) and are almost the same as the pristine Au NCs (Fig. 3b). It indicated the coexistence of Au(0) and Au(I), consistent with the chemical structure of the Au NCs. After two peaks separated into Au $4f_{5/2}$ (87.65 eV) and Au $4f_{7/2}$ (84.00 eV) of Au(0) and Au $4f_{5/2}$ (88.10 eV) and Au $4f_{7/2}$ (84.43 eV) of Au(I), the calculated Au(0) : Au(I) ratio was 50.8 : 49.2, which well matched the pristine Au NCs (Table S1, ESI†). It proved that the chemical structure of the Au NCs was maintained in fibrous-Au-GG. The absorption spectra in Fig. 3c show that the Au NCs in fibrous-Au-GG exhibited two main peaks at 450 nm and 660 nm, which were attributed to the intraband and interband transition of pure Au NCs, respectively. Whereas, fibrous-GG had no characteristic absorption peak in the UV-Vis range. Thus, it is proved that the annealing treatment of gellan gum did not bias the physicochemical nature of the Au NC. Moreover, without the annealing process, the Au-GG hydrogel and the GG hydrogel cross-linked by $Ca^{2+}$ were also prepared, which were proven by the uniform distribution of Ca element (Fig. S4a and b, ESI†). The gellan gum hydrogel has a homogeneously porous structure. Combined with the images in Fig. 2, the ultra-small Au NCs can be successfully coupled with gellan gum without changing the intrinsic characteristics of gellan gum. Through annealing, a gold nanocluster decorated fibrous substrate formed by hydrogen bonding and coordination could be obtained.

Then, the mechanical properties of the substrate were examined. As the compress stress–strain curves in Fig. 4a show, when compressed to 40%, the fibrous substrates displayed higher stress than the hydrogel without annealing. Among these substrates, fibrous-Au-GG was the strongest with 0.45 MPa. The calculated compression modulus was 0.43 MPa, higher than the value of 0.36 MPa for fibrous-GG, followed by 0.12 MPa for the Au-GG hydrogel and 0.04 MPa for the GG hydrogel (Fig. 4b). The results demonstrated that the fibrous substrates are more rigid than the hydrogel, and indicated that the dense network in the fibrous substrates contributes to the rigidity. The enhanced rigidity of fibrous-Au-GG may be attributed to the interactions

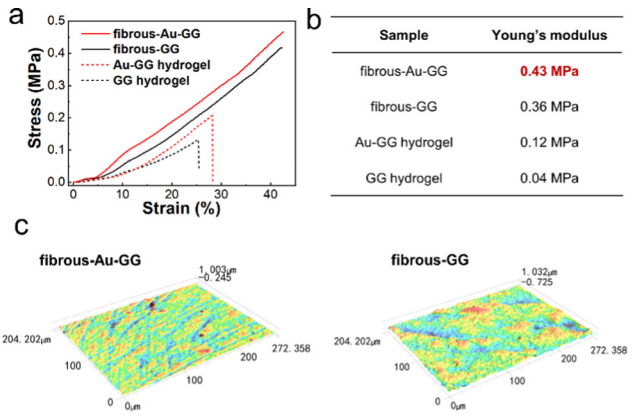


Fig. 4 (a) Compression stress–strain curves and (b) Young's modulus of different fibrous substrates and hydrogels. (c) Images of the surface morphology of fibrous-Au-GG and fibrous-GG.

between the Au NCs and gellan gum, which constrain the mobility of the filamentous aggregates.

The surface morphologies of different substrates were observed by a laser scanning microscope (Fig. 4c). Bumpy strips were present in fibrous-Au-GG. The average roughness is 0.03 μm, lower than that of fibrous-GG of 0.11 μm. The result was consistent with the observations in the SEM images. We speculate that the Au NCs are involved in cross-linking and restrict the motion of filamentous aggregates, resulting in a denser fibrous network. However, the hydrogels did not display lots of bumps, because they did not anneal and therefore do not contain filamentous aggregates (Fig. S5, ESI†). Thus, the incorporated Au NCs can impart the rigidity and a fibril surface, which provide mechanistic cues to modulate cellular behaviour.

In addition, the Au NCs with photothermal properties can endow fibrous-Au-GG with photothermal conversion capability. The 660 nm laser at a power density of 1.65 W $cm^{-2}$ was applied to exert and evaluate the photothermal effect of fibrous-Au-GG. As shown in Fig. 5a and Video S1 (ESI†), the temperature of the irradiated areas increased to 35 °C rapidly within 3 min, reached a plateau and gradually decreased after the laser was turned off. The plateau meant that thermal equilibrium was achieved between the photothermal conversion and environmental thermal dissipation at such an elevated temperature. As the

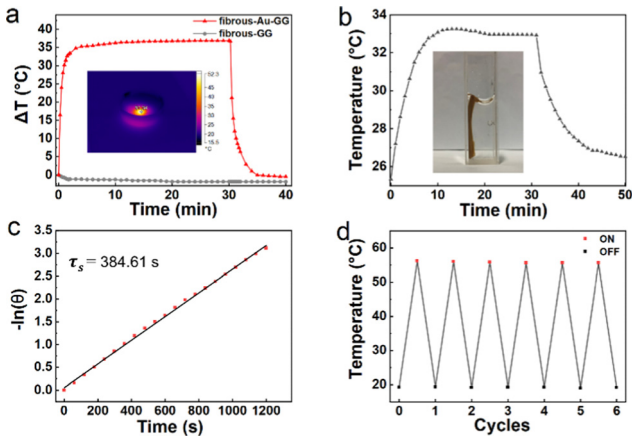


Fig. 5 (a) Photothermal heating–cooling curves of fibrous-Au-GG and fibrous-GG. Insert: Thermograph of fibrous-Au-GG. (b) Photothermal heating–cooling curves and photograph of fibrous-Au-GG in water. (c) The negative natural logarithm of temperature *versus* time from the cooling period. (d) Temperature change of fibrous-Au-GG for six heating–cooling cycles.

environmental thermal dissipation increased significantly with the rise of the sample temperature, the location of the plateau qualitatively indicated that the high efficiency and fast response of photothermal conversion was well inherited by fibrous-Au-GG. As the control, almost no temperature change of fibrous-GG was observed upon irradiation. Then, 1 cm × 2 cm fibrous-Au-GG was immersed into 2 mL of water to obtain the heating–cooling curves (Fig. 5b). From the cooling stage, the system time constant ($\tau_s$) was obtained as 384.61 s. Then, the photothermal conversion efficiency of fibrous-Au-GG was calculated to 31.2% (Fig. 5c). Thus, fibrous-Au-GG could convert light energy into heat. More importantly, after 6 on/off irradiation cycles, the peak temperature scarcely fluctuated, meaning that fibrous-Au-GG has good photothermal stability from a macroscopic and phenomenal view (Fig. 5d). From the SEM image in Fig. S6 (ESI†), the structural integrity of the filamentous aggregates was highly maintained. Meanwhile, the Au(0) : Au(I) ratio of fibrous-Au-GG after irradiation was the same as before irradiation (Fig. S7a, ESI†). The characteristic absorption peaks of the Au NCs were well maintained after irradiation (Fig. S7b, ESI†). As a result, fibrous-Au-GG processes good thermal stability with light-response from a microscopic view.

The structure of the ionic cross-links and the function of light-response permit fibrous-Au-GG to load and release proteins. Owing to the carboxyl groups presented in FITC-whey proteins, these proteins can be also loaded by $Ca^{2+}$ ion crosslinking, in the same way as glutathione-coated Au NCs (Fig. S8, ESI†). As shown in Fig. 6a, the aggregates of the filamentous structure with small pores were observed from fibrous-Au/protein-GG, which aligned with that of fibrous-Au-GG. The absorption peak at 480 nm and the emission peak at 520 nm prove the successful loading of FITC-whey proteins (Fig. 6b). Thus, green fluorescence can be observed from fibrous-Au/protein-GG (Fig. 6c). Under 660 nm irradiation for 3 min, the temperature of fibrous-Au/protein-GG reached 48.5 °C (Fig. 6d). Thus, the physical morphology and photothermal properties of fibrous-Au-GG were both well maintained after protein loading, which satisfied the prerequisite of the remote light-triggered release of proteins.

FITC emission was used to monitor protein release in response to light-generated heat. Before the test, we optimized the irradiation dose. As shown in Fig. S9 (ESI†), at a power density of 0.5 W $cm^{-2}$, the maximum temperature of fibrous-Au/protein-GG could increase to 23.5 °C. While for the power density of 0.8 W $cm^{-2}$, the maximum temperature rose to 38.3 °C, which is safe to prevent protein denaturation and cell

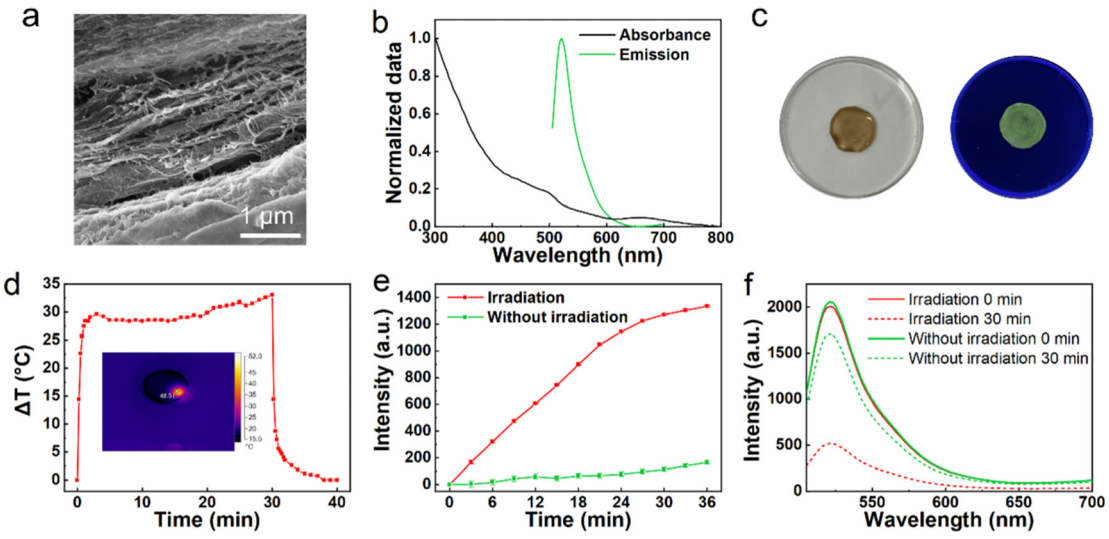


Fig. 6 (a) The SEM image of fibrous-Au/protein-GG. (b) Normalized absorption and emission spectra of fibrous-Au/protein-GG. (c) Bright field and fluorescent images of fibrous-Au/protein-GG. (d) Photothermal heating–cooling curve and thermograph of fibrous-Au/protein-GG. (e) Fluorescence intensities of FITC-whey proteins released from immersed fibrous-Au/protein-GG with and without irradiation. (f) Fluorescence intensities of fibrous-Au/protein-GG with and without irradiation at 0 and 30 min, respectively.

 

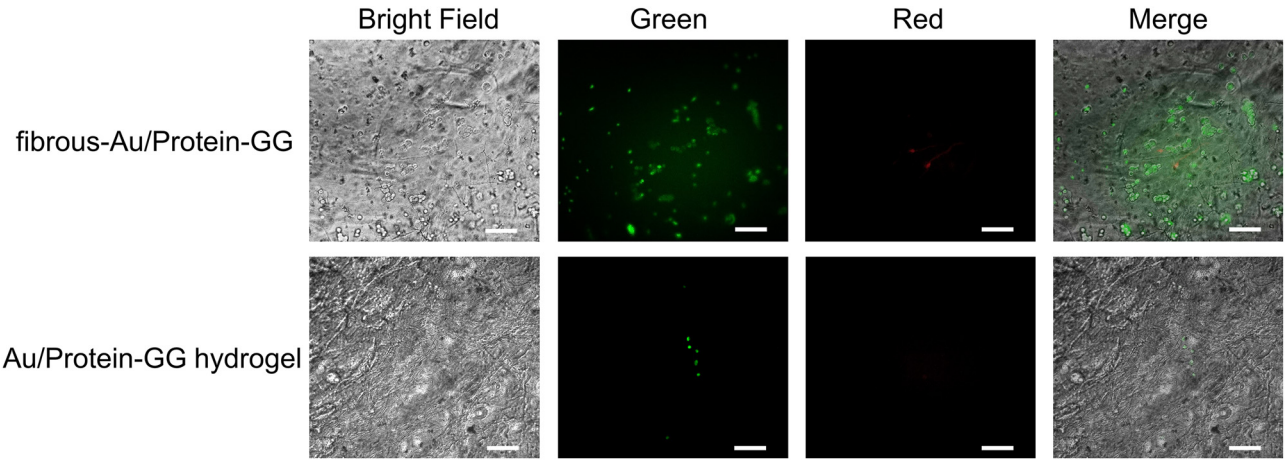


Fig. 7 Viability of MG-63 cells adhered on fibrous-Au/protein-GG and Au/protein-GG hydrogels. The calcein emitted green fluorescence and the PI emitted red fluorescence (scale bar, 100 μm).

death. Under the irradiation dose, the gradually enhanced FITC emission was observed from the PBS solution by extending the irradiation time, which revealed the sustained protein release from fibrous-Au/protein-GG (Fig. 6e). After 30 min of laser irradiation, a significant reduction in the rate of fluorescence increase may indicate nearly complete protein release in fibrous-Au/protein-GG. Without irradiation, the very slow release of protein was observed during the immersing process. The slight background leakage of protein may result from ion exchange in the PBS.[14] Correspondingly, the 520 nm emission of the irradiated area in fibrous-Au/protein-GG was significantly decreased (Fig. 6f), while there was a slight decrease in the emission for fibrous-Au/protein-GG without irradiation. Through comparison, fibrous-Au/protein-GG exhibited fast and enhanced protein release in an on-demand way when triggered by light.

As whey protein can promote bone cell proliferation,[50] we then evaluated whether cell proliferation benefits from the controllable protein release of fibrous-Au/protein-GG. Because cell adhesion on the substrate plays an important role in further cell proliferation, MG-63 cells were seeded on different substrates. After 12 h of incubation, the cell adhesion was assessed. The captured images in Fig. 7 verified the adhesion of MG-63 cells on fibrous-Au/protein-GG. Cell viability was analysed by live-dead cell staining. A large amount of the adherent cells were alive, which could be labelled by calcein-AM that showed green fluorescence. The dead cells were labelled by PI and showed red fluorescence. The high viability of the adherent cells was confirmed. Meanwhile, a similar cell adhesion was observed on fibrous-GG and fibrous-Au-GG (Fig. S10, ESI†). In contrast, a poor cell adhesion was observed from Au/protein-GG hydrogel, also from GG hydrogel and Au-GG hydrogel (Fig. S11, ESI†). The difference in the adhesion state of the cells is largely due to the rigidity of the substrate. The results indicated that the structure of fibrous-Au/protein-GG can significantly improve cell adhesion.

We then irradiated the substrate to release whey protein. After incubation for one day, cell growth was shown on fibrous-Au/protein-GG with or without irradiation, reflecting the high biocompatibility (Fig. 8a). But there was an apparent higher cell number on fibrous-Au/protein-GG with irradiation compared to that without irradiation. In the enlarged images, these cells displayed flattened and well-spread morphology. For Au/protein-GG hydrogel, although the cells grew after irradiation, their population did not increase significantly over time. Most of them

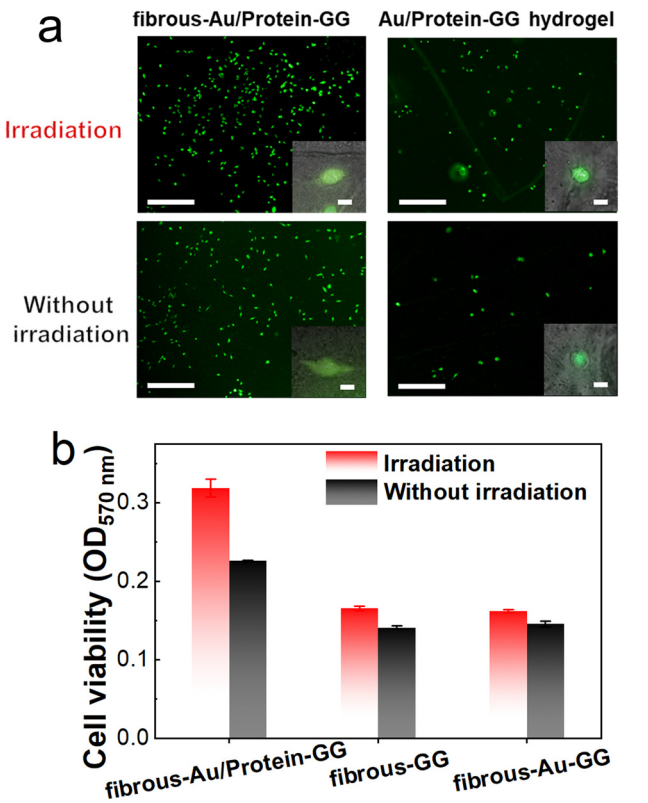


Fig. 8 (a) Fluorescent images of MG-63 cells on fibrous-Au/protein-GG and Au/protein-GG hydrogels with and without irradiation (scale bar, 500 μm). Insert: Magnified fluorescent images of MG-63 cells (scale bar, 20 μm). (b) MTT assay of cells grown on fibrous-Au/protein-GG, fibrous-GG and fibrous-Au-GG with and without irradiation, respectively.

still appeared round. In addition, by the MTT assay, the absorption intensity at 570 nm with irradiation was 35% higher than that of non-irradiation, confirming the increased proliferation (Fig. 8b). However, for fibrous-GG and fibrous-Au-GG, the same cell proliferation was observed in irradiation and non-irradiation groups. Thus, the bioactive whey protein release from fibrous-Au/protein-GG by photothermal conversion of the Au NCs, can influence the cell proliferation. Fibrous-Au/protein-GG well supports photo-modulated cellular growth.

## 4. Conclusions

In summary, we successfully prepared a light-responsive fibrous substrate integrated with photothermal Au NCs to regulate cell growth. Through a suitable annealing process, the ultra-small Au NCs were simply incorporated to filamentous aggregates of gellan gum. Then, the organic ligands of the Au NCs were $Ca^{2+}$ cross-linked with gellan gum and bioactive whey protein to form a biofunctional substrate. The incorporated Au NCs enhanced the rigidity of the fibrous substrate and tightened the arrangement of the fibrous structures, which offers a suitable surface to promote cell adhesion. More importantly, the Au NCs act not only as reinforcing agents but also as effective photothermal agents. A burst light-triggered release of whey protein from the fibrous substrate was controlled by irradiating the photothermal Au NCs. The biological activity of the loaded whey protein improved cellular growth on the platform. Owing to its optical function and low cytotoxicity, the fibrous substrate has the potential to remotely modulate cell proliferation. Therefore, the photo-enabled cell culture system is expected to be used in a wide range of biological applications including tissue engineering and drug delivery.

## Author contributions

B. L.: data curation, methodology, investigation, validation and writing – review & editing. Y. K.: formal analysis, investigation and writing – review & editing. X. W.: conceptualization, formal analysis, supervision, funding acquisition, project administration and writing – review & editing. P. Z.: data curation and methodology. L. L.: conceptualization, supervision, resources and writing – review & editing.

## Conflicts of interest

There are no conflicts to declare.

## Acknowledgements

This work was financially supported by the National Natural Science Foundation of China (22177012 and 51973016) and the Fundamental Research Funds for the Central Universities (FRF-IDRY-20-026 and 00007485).

## References

1 J. P. Wojciechowski and M. M. Stevens, *Science*, 2021, **374**, 825–826.
2 G. S. Hussey, J. L. Dziki and S. F. Badylak, *Nat. Rev. Mater.*, 2018, **3**, 159–173.
3 G. Huang, F. Li, X. Zhao, Y. Ma, Y. Li, M. Lin, G. Jin, T. J. Lu, G. M. Genin and F. Xu, *Chem. Rev.*, 2017, **117**, 12764–12850.
4 A. D. Theocharis, S. S. Skandalis, C. Gialeli and N. K. Karamanos, *Adv. Drug Delivery Rev.*, 2016, **97**, 4–27.
5 S. Hinderer, S. L. Layland and K. Schenke-Layland, *Adv. Drug Delivery Rev.*, 2016, **97**, 260–269.
6 A. Fernández-Colino, F. J. Arias, M. Alonso and J. C. Rodríguez-Cabello, *Biomacromolecules*, 2014, **15**, 3781–3793.
7 H. Chen, Y. S. Lui, Z. W. Tan, J. Y. H. Lee, N. S. Tan and L. P. Tan, *Adv. Healthcare Mater.*, 2019, **8**, 1801378.
8 Q. Zhang, X. Wang, Y. Cong, Y. Kang, Z. Wu and L. Li, *ACS Appl. Mater. Interfaces*, 2022, **14**, 12674–12683.
9 M. D. Davidson, M. E. Prendergast, E. Ban, K. L. Xu, G. Mickel, P. Mensah, A. Dhand, P. A. Janmey, V. B. Shenoy and J. A. Burdick, *Sci. Adv.*, 2021, **7**, eabi8157.
10 A. A. Abalymov, C. A. B. Santos, L. Van der Meeren, D. Van de Walle, K. Dewettinck, B. V. Parakhonskiy and A. G. Skirtach, *Adv. Mater. Interfaces*, 2021, **8**, 2002202.
11 L. Zhang, J. Fang, L. Fu, L. Chen, W. Dai, H. Huang, J. Wang, X. Zhang, Q. Cai and X. Yang, *Chem. Eng. J.*, 2021, **422**, 130428.
12 R. J. Wade and J. A. Burdick, *Nano Today*, 2014, **9**, 722–742.
13 X. N. Zhang, Y. J. Wang, S. Sun, L. Hou, P. Wu, Z. L. Wu and Q. Zheng, *Macromolecules*, 2018, **51**, 8136–8146.
14 Z. Clapacs, C. L. ONeill, P. Shrimali, G. Lokhande, M. Files, D. D. Kim, A. K. Gaharwar and J. S. Rudra, *Biomacromolecules*, 2022, **23**, 1183–1194.
15 Y. M. Shin, T. G. Kim, J.-S. Park, H.-J. Gwon, S. I. Jeong, H. Shin, K.-S. Kim, D. Kim, M.-H. Yoon and Y.-M. Lim, *J. Mater. Chem. B*, 2015, **3**, 2732–2741.
16 R. J. Wade and J. A. Burdick, *Mater. Today*, 2012, **15**, 454–459.
17 J. K. Sahoo, M. A. VandenBerg and M. J. Webber, *Adv. Drug Delivery Rev.*, 2018, **127**, 185–207.
18 P. Atienza-Roca, D. C. Kieser, X. Cui, B. Bathish, Y. Ramaswamy, G. J. Hooper, A. N. Clarkson, J. Rnjak-Kovacina, P. J. Martens, L. M. Wise, T. B. F. Woodfield and K. S. Lim, *Biomater. Sci.*, 2020, **8**, 5005–5019.
19 D. A. Cook, S. W. Fellgett, M. E. Pownall, P. J. O'Shea and P. G. Genever, *Stem Cell Res.*, 2014, **12**, 415–427.
20 L. Xu, S. Gao, R. Zhou, F. Zhou, Y. Qiao and D. Qiu, *Adv. Mater.*, 2020, **32**, 1907491.
21 C. Zhang, K. Wang, X. Guo and Y. Tang, *J. Mater. Chem. C*, 2022, **10**, 2600–2607.
22 E. Cheah, Z. Wu, S. S. Thakur, S. J. O'Carroll and D. Svirskis, *J. Controlled Release*, 2021, **332**, 74–95.
23 C. Li, K. Feng, N. Xie, W. Zhao, L. Ye, B. Chen, C.-H. Tung and L.-Z. Wu, *ACS Appl. Nano Mater.*, 2020, **3**, 5070–5078.
24 J. S. Basuki, F. Qie, X. Mulet, R. Suryadinata, A. V. Vashi, Y. Y. Peng, L. Li, X. Hao, T. Tan and T. C. Hughes, *Angew. Chem., Int. Ed.*, 2017, **56**, 966–971.

 

25 X. Fu, Y. Huang, H. Zhao, E. Zhang, Q. Shen, Y. Di, F. Lv, L. Liu and S. Wang, *Adv. Mater.*, 2021, **33**, 2102570.
26 H. Sun and K. S. Schanze, *ACS Appl. Mater. Interfaces*, 2022, **14**, 20506–20519.
27 H. Lu, Y. Huang, F. Lv, L. Liu, Y. Ma and S. Wang, *CCS Chem.*, 2021, **3**, 1296–1305.
28 W. Li, Z. Yan, J. Ren and X. Qu, *Chem. Soc. Rev.*, 2018, **47**, 8639–8684.
29 C.-M. Chen, Y.-J. Huang and K.-H. Wei, *Nanoscale*, 2014, **6**, 5999–6008.
30 C.-M. Chen, C.-M. Liu, K.-H. Wei, U. S. Jeng and C.-H. Su, *J. Mater. Chem.*, 2012, **22**, 454–461.
31 J. You, J. S. Heo, J. Kim, T. Park, B. Kim, H.-S. Kim, Y. Choi, H. O. Kim and E. Kim, *ACS Nano*, 2013, **7**, 4119–4128.
32 J. Kim, E. Lee, Y. Hong, B. Kim, M. Ku, D. Heo, J. Choi, J. Na, J. You, S. Haam, Y.-M. Huh, J.-S. Suh, E. Kim and J. Yang, *Adv. Funct. Mater.*, 2015, **25**, 2260–2269.
33 Q. Yao, Z. Wu, Z. Liu, Y. Lin, X. Yuan and J. Xie, *Chem. Sci.*, 2021, **12**, 99–127.
34 S. Zhou, Y. Duan, K. Liu and R. H. A. Ras, *J. Mater. Chem. C*, 2022, **10**, 10001–10008.
35 X. Jiang, X. Wang, C. Yao, S. Zhu, L. Liu, R. Liu and L. Li, *J. Phys. Chem. Lett.*, 2019, **10**, 5237–5243.
36 S. K. Katla, J. Zhang, E. Castro, R. A. Bernal and X. Li, *ACS Appl. Mater. Interfaces*, 2018, **10**, 75–82.
37 X. Kang, H. Chong and M. Zhu, *Nanoscale*, 2018, **10**, 10758–10834.
38 X. Liu, Y. Yang, X. Wang, X. Liu, H. Cheng, P. Wang, Y. Shen, A. Xie and M. Zhu, *J. Mater. Chem. B*, 2021, **9**, 6396–6405.
39 H. Qin, T. Zhang, H.-N. Li, H.-P. Cong, M. Antonietti and S.-H. Yu, *Chem*, 2017, **3**, 691–705.
40 Y. Li, Y. Song, X. Zhang, T. Liu, T. Xu, H. Wang, D.-E. Jiang and R. Jin, *J. Am. Chem. Soc.*, 2022, **144**, 12381–12389.
41 N. Yang, Y. Kang, Y. Cong, X. Wang, C. Yao, S. Wang and L. Li, *Adv. Mater.*, 2022, 2208349.
42 X. Wang, J. Xia, C. Wang, L. Liu, S. Zhu, W. Feng and L. Li, *ACS Appl. Mater. Interfaces*, 2017, **9**, 44856–44863.
43 M. Zhu, Q. Yao, Z. Liu, J. Liu, M. Liu, M. Long and J. Xie, *J. Phys. Chem. Lett.*, 2022, **13**, 7722–7730.
44 Y. Cong, X. Wang, C. Yao, Y. Kang, P. Zhang and L. Li, *ACS Appl. Mater. Interfaces*, 2022, **14**, 4532–4541.
45 M.-M. Xu, T.-T. Jia, B. Li, W. Ma, X. Chen, X. Zhao and S.-Q. Zang, *Chem. Commun.*, 2020, **56**, 8766–8769.
46 S. Zhu, X. Wang, Y. Cong, L. Liu and L. Li, *ACS Appl. Mater. Interfaces*, 2021, **13**, 19360–19368.
47 A. Paściak, R. Marin, L. Abiven, A. Pilch-Wróbel, M. Misiak, W. Xu, K. Prorok, O. Bezkrovnyi, Ł. Marciniak, C. Chanéac, F. Gazeau, R. Bazzi, S. Roux, B. Viana, V.-P. Lehto, D. Jaque and A. Bednarkiewicz, *ACS Appl. Mater. Interfaces*, 2022, **14**, 33555–33566.
48 X. Li, F. Fang, B. Sun, C. Yin, J. Tan, Y. Wan, J. Zhang, P. Sun, Q. Fan, P. Wang, S. Li and C.-S. Lee, *Nanoscale Horiz.*, 2021, **6**, 177–185.
49 E. R. Morris, K. Nishinari and M. Rinaudo, *Food Hydrocolloids*, 2012, **28**, 373–411.
50 M. Dziadek, K. Charuza, R. Kudlackova, J. Aveyard, R. D'Sa, A. Serafim, I.-C. Stancu, H. Iovu, J. G. Kerns, S. Allinson, K. Dziadek, P. Szatkowski, K. Cholewa-Kowalska, L. Bacakova, E. Pamula and T. E. L. Douglas, *Mater. Des.*, 2021, **205**, 109749.